

# A Swift and Omnidirectional Formation Approach based on Hierarchical Reorganization

Yuzhu Li, Wei Dong\*.

**Abstract**—Current formations commonly rely on invariant hierarchical structures, such as predetermined leaders or enumerated formation shapes. These structures could be unidirectional and sluggish, constraining their adaptability and agility when encountering cluttered environments. To surmount these constraints, this work proposes an omnidirectional affine formation approach with hierarchical reorganizations. We first delineate the critical conditions requisite for facilitating hierarchical reorganizations within formations, which informs the development of the omnidirectional affine criterion. Central to our approach is the fluid leadership and authority redistribution, for which we develop a minimum time-driven leadership evaluation algorithm and a power transition control algorithm. These algorithms facilitate autonomous leader selection and ensure smooth power transitions, enabling the swarm to adapt hierarchically in alignment with the external environment. Furthermore, we deploy a power-centric topology switching mechanism tailored for the dynamic reorganization of in-team connections. Finally, simulations and experiments demonstrate the performance of the proposed method. The formation successfully performs several hierarchical reorganizations, with the longest reorganization taking only 0.047s. This swift adaptability allows five aerial robots to carry out complex tasks, including executing swerving movements and navigating through hoops at velocities up to 1.9m/s.

**Index Terms**—Hierarchical Reorganization, Omnidirectional Affine Formation, Leader Selection, Swarm

## I. INTRODUCTION

Aerial robots have garnered growing scholarly interest in recent years due to their vast potential for application in collaborative tasks, including exploration [1], [2], inspection [3], fire rescue [4]. Swarm formations, in particular, exhibit remarkable performance in self-organization, survivability, and collaborative task execution [5]. In complex environments, adopting variable formations during flight becomes crucial for maintaining optimal mobility and flexibility [6].

The architectural frameworks facilitating formation reorganization can principally be categorized into democratic and autocratic. In democratic formations, the entire group is generally regarded as a unified entity, each planning their actions based on collective information and influencing the overall formation. For instance, in [7], the formation is conceptualized as a virtual rigid body, which allows for versatile transformations of various formation patterns by adjusting the relative orientations and positions of individual aerial robots with a virtual center. This approach facilitates

the execution of complex tasks, such as navigating through cluttered buildings, dense forests, or disaster-stricken sites. However, this method relies on a virtual structure to govern the formation's pattern, demanding real-time computation of transfer vectors for each individual within the formation. As the scale of aerial robots increases, the complexity of democratic reconfiguration correspondingly escalates, thereby diminishing the formation's flexibility and robustness.

Conversely, autocratic formation reorganization relies on a subset of agents within the formation. By hierarchically distributing the power among different individuals, certain members exert influence over the overall formation pattern, facilitating formation reorganization. For example, Ref. [8] introduces an affine formation method within a leader-follower framework. This method achieves comprehensive formation changes through the strategic positioning of the leader, enabling seamless continuous transitions, including translation, rotation, contraction, and deformation. However, the autocratic formations' leaders remain unchanged, forming a unidirectional affine transformation. This configuration may pose challenges when the swarm needs to execute sharp turns or large-angle maneuvers, potentially limiting its flexibility.

Given the abovementioned challenges, our approach draws inspiration from the swerving and hierarchical formation movements observed in starling clusters, as explored in [9], [10]. Starling flocks typically feature one or multiple leaders, with the formation's internal framework exhibiting a structure between democratic and autocratic paradigms. Building on this, the cluster dynamically adjusts its movement patterns, leading to hierarchical reorganization within the formation. In light of this natural phenomenon, we introduce an omnidirectional affine formation, leveraging hierarchical reorganizations to enhance the flexibility of formations and in-team coordination.

Firstly, we elucidate the essential conditions for facilitating hierarchical reorganizations. Following this, we introduce a minimum time-driven leadership evaluation algorithm designed to streamline autonomous leader selection, thereby optimizing decision-making processes within the formation. With a focus on the seamless redistribution of leadership, a power transition control algorithm is proposed to ensure smooth authority redistribution. To enhance the formation's internal synchrony, we deploy a power-centric topology switching mechanism tailored for the dynamic reorganization of in-team connections.

The main contributions of the paper are as follows:

- 1) A novel omnidirectional affine formation strategy

The authors are with the State Key Laboratory of Mechanical System and Vibration, School of Mechanical Engineering, Shanghai Jiao Tong University, Shanghai 200240, China (e-mail: {yuzhu\_0222, dr.dongwei}@sjtu.edu.cn).

based on hierarchical reorganizations is proposed to efficiently improve the formation's flexibility and coordination.

- 2) A power transition control algorithm is presented, which employs a designed power transfer function to achieve synchronized authority redistribution.
- 3) A power-centric topology switching algorithm is put forward, aimed at mitigating disturbances caused by followers to further enhance the formation's internal synchrony.

The remainder of this paper is organized as follows. Related works are introduced in Section II. Preliminaries and problem formulation are given in Section III. The specific methodology is described in Section IV, which contains definitions for omnidirectional affine formation, a minimum time-driven leadership evaluation algorithm, a power transition control algorithm and a power-centric topology switch strategy. Verification is carried out in Section V, while Section VI concludes the paper.

## II. RELATED WORKS

The related works are segmented into three sections. The first section explores algorithms dedicated to dynamic leader selection, reflecting on the existing criteria for fluid leadership. Subsequently, the second section delves into the methodologies governing hierarchical formation control, presenting a detailed overview of established approaches. The final section critically evaluates the role of topological switching, emphasizing its critical importance in hierarchical formation control.

### A. Dynamic Leader Selection

Researchers have made significant progress in leader selection to enhance various aspects of swarm formation performance [11], [12]. The focus is generally on selecting leaders based on specific task requirements. For instance, Ref. [13] formulates the leader selection problem as a fast mixed convex optimization problem, aiming to minimize convergence time by determining the appropriate number of leaders; Ref. [14] selects leaders based on criteria such as convergence speed and control energy. These studies underscore the importance of leader selection in optimizing swarm formation performance by considering factors like convergence time and task-specific requirements. However, these approaches are committed to static leader selection before initiating a single task. In practical situations, dynamic leader selection has been shown to improve the overall performance of a robot team compared to a static leader [15].

Dynamic leader selection involves changes in leader roles during the task due to various factors. On the one hand, this includes human or human base station influence over the robotic system. For instance, Ref. [16]-[18] improve communication quality with the base station by online leader selection in the swarm, and Ref. [19] proposes using human-robot trust as a dynamic criterion

for leader selection, reducing task completion time and formation errors compared to non-leader switching strategies. However, these methods are constrained by the quality of human-machine communication and the accuracy of human judgment on the swarm's current state, making them unsuitable for autonomous systems.

Considering the autonomy of the swarm, another aspect of dynamic leader selection is the influence of the external environment on the robotic swarm. For example, Ref. [20] suggests a method for reselecting leaders in case of leader failure in environments with dense obstacles. To address the leader trapping issue caused by different probabilities of encountering obstacles for different roles within the formation, Ref. [21] introduces an emotion-based model for leader selection. This model allows the team to autonomously reselect a leader when trapped and continue moving towards the goal. However, while this method can increase the probability of individual escape, it does not guarantee the successful escape of the entire swarm.

### B. Hierarchical Formation Control

The hierarchical formation control can draw inspiration from collective movements observed in biological systems. For instance, the migration of bird flocks and mammal herds utilizes a leader-follower strategy to address the capability disparities among individuals [22], [23]. Numerous researchers have investigated formation control problems using leader-follower strategies [24], [25]. They have identified various formation structures, such as single-leader formation [26]-[28], multi-leader formation [29], [30], and virtual leader formation [31], [32]. Multi-leader structures, which allow for affine formation through adjusting leaders' relative positions, have gained particular interest compared to single-leader and virtual-leader formation.

To achieve affine transformations, Ref. [33] explores the sufficient and necessary conditions for realizing affine formations based on graph theory. Building on this, Ref. [8] proposes a control method for leader-follower formations based on affine transformation, demonstrating through simulations that the following error of followers converges exponentially. Furthering this approach, Ref. [34] introduces a hierarchical affine control algorithm to achieve formation control under conditions of non-global information, thereby enhancing the robustness of the control strategy. However, practical scenarios often involve communication delays among multiple agents, adversely affecting the effectiveness of the methods mentioned above.

Addressing the communication delays, several approaches have been proposed in recent research [35], [36]. One approach proposes using adaptive distributed observers to estimate the leader's system matrix and state for each follower. By building a distributed controller, the approach achieves output consensus between leaders and followers [37]. Another approach focuses on the affine formation control of multi-agent systems with prescribed convergence times, which is accomplished by designing a distributed

continuous control algorithm [38]. However, these control algorithms are all based on static and unidirectional structures, and research on formation control under hierarchical reorganizations is still in its infancy.

### C. Topology Switching for Hierarchical Formation

Research has indicated that internal topology switching within a formation can enhance multiple capabilities of the formation. For example, Ref. [39] enhances the resilience of a swarm by designing internal topology transitions; Ref. [40] proposes an optimal rigidity graph-based topology optimization algorithm to reduce the communication complexity of formations, thereby extending the network's lifespan; Ref. [41] designs smooth transitions in communication to ensure security during topological changes. The introduction of dynamic topology switching into formation control has added new variables [42], [43], making this area a subject of extensive research.

Considering the control problems of formations under topology switching, Ref. [44] proposes the necessary and sufficient conditions for achieving time-varying formation tracking under topology transitions, and the system's stability has been verified experimentally. Building on this, Ref. [45] presents a distributed control algorithm using neighboring positions and velocities during the topology transition process when weak connections exist in the communication topology among individuals in the swarm. Considering different formation structures, the problem of hierarchical formation control with topology switching has been further explored.

To investigate the impact of topology switching on the control of hierarchical formation structures, Ref. [46] conducts a controllability analysis of hierarchical formations under topology switching. Based on this, Refs. [47], [48] study the control issues of leaders and followers during topology transitions. Furthermore, Refs. [8], [33] explore the relationship between hierarchical control issues in affine formation and topological structures. Considering the introduction of hierarchical reorganization strategies in these problems, Ref. [14] optimizes the formation of topological structures to reduce communication costs while improving convergence speed. However, no method has yet explored the impact of topology switching on formation control during hierarchical reorganizations.

## III. PRELIMINARIES AND PROBLEM STATEMENT

### A. Basic Graph and Formation Theory

Consider a group of  $n$  mobile agents in  $\mathbf{R}^d$  where  $d > 2$  and  $n \geq d + 1$ . Let  $\mathbf{p}_i \in \mathbf{R}^d$  be the position of agent  $i$  and  $\mathbf{p} = [\mathbf{p}_1^T, \dots, \mathbf{p}_n^T]^T \in \mathbf{R}^{dn}$  be the configuration of all the agents. The interaction between the agents is modeled by a graph  $\mathcal{G}(\mathcal{V}, \mathcal{E})$  where  $\mathcal{V} = \{1, 2, \dots, n\}$  is the node set and  $\mathcal{E} \subseteq \mathcal{V} \times \mathcal{V}$  is the edge set. For a digraph, the edge set consists of directed edges  $(j, i)$ , where node  $j$  is the tail node and node  $i$  is the head node. Node  $j$  is called the in-neighbor of node  $i$ , while node  $i$  is called the out-neighbor

of node  $j$  and  $\mathcal{N}_i := \{j | (j, i) \in \mathcal{E}\}$  denotes the in-neighbor set for agent  $i$ . In a digraph,  $(j, i) \in \mathcal{E} \neq (i, j) \in \mathcal{E}$ . An orientation of an undirected graph is the assignment of a direction to each undirected edge. An oriented graph is an undirected graph together with an orientation. The incidence matrix  $\mathbf{D} \in \mathbf{R}^{m \times n}$  of an oriented graph is the  $\{0, \pm 1\}$ -matrix with rows indexed by edges and columns.

A formation, denoted as  $(\mathcal{G}, \mathbf{p})$ , is the graph  $\mathcal{G}$  with its vertex  $i$  mapped to point  $\mathbf{p}_i$ . Without loss of generality, suppose the first  $n_l$  agents are leaders and the rest  $n_f = n - n_l$  agents are followers. Let  $\mathcal{V}_l = 1, \dots, n_l$  and  $\mathcal{V}_f = \mathcal{V} \setminus \mathcal{V}_l$  be the sets of leaders and followers, respectively. The positions of the leaders and followers are denoted as  $\mathbf{p}_l = [\mathbf{p}_1^T, \dots, \mathbf{p}_{n_l}^T]^T$  and  $\mathbf{p}_f = [\mathbf{p}_{n_l+1}^T, \dots, \mathbf{p}_n^T]^T$ , respectively.

### B. Affine Formation Maneuver Control

For formation  $(\mathcal{G}, \mathbf{p})$ , a stress is denoted as  $\{\omega_i^j\}_{(i,j) \in \mathcal{E}}$ . According to [49], a stress is called an equilibrium stress if it satisfies

$$\sum_{j \in \mathcal{N}_i} \omega_i^j (\mathbf{p}_j - \mathbf{p}_i) = 0, \quad i \in \mathcal{V} \quad (1)$$

To simplify the expression of Eq.(1), the stress matrix is defined as  $\mathbf{\Omega} \in \mathbf{R}^{n \times n}$  which satisfies

$$\begin{cases} 0, & i \neq j, (i, j) \notin \mathcal{E} \\ -\omega_i^j, & i \neq j, (i, j) \notin \mathcal{E} \\ \sum_{k \in \mathcal{N}_i} \omega_i^k, & i = j \end{cases} \quad (2)$$

Then, the Eq.(1) can be expressed in a matrix form as

$$(\mathbf{\Omega} \otimes \mathbf{I}_d) \mathbf{p} = \mathbf{0} \quad (3)$$

In this paper, denote  $\bar{\mathbf{\Omega}} = \mathbf{\Omega} \otimes \mathbf{I}_d$  for notational simplicity. Partition  $\bar{\mathbf{\Omega}}$  according to the partition of leaders and followers as  $\bar{\mathbf{\Omega}} = \begin{bmatrix} \bar{\mathbf{\Omega}}_{ll} & \bar{\mathbf{\Omega}}_{lf} \\ \bar{\mathbf{\Omega}}_{fl} & \bar{\mathbf{\Omega}}_{ff} \end{bmatrix}$ . The stress condition for affine localizability is as follows:

**Lemma III.1.** (Stress Condition for Affine Localizability [8]) *The nominal formation  $(\mathcal{G}, \mathbf{r})$  is affinely localizable if and only if  $\bar{\mathbf{\Omega}}_{ff}$  is nonsingular. When  $\bar{\mathbf{\Omega}}_{ff}$  is nonsingular, for any  $\mathbf{p} = [\mathbf{p}_l^T, \mathbf{p}_f^T]^T \in \mathcal{A}(\mathbf{r})$ ,  $\mathbf{p}_f$  can be uniquely calculated as  $\mathbf{p}_f = -\bar{\mathbf{\Omega}}_{ff}^{-1} \bar{\mathbf{\Omega}}_{fl} \mathbf{p}_l$ .*

### C. Problem Statement

During the traversal of an aerial formation through any environment  $\mathbf{E}$ , the complexity of  $\mathbf{E}$  imposes constraints on the traversal direction. Building on this, agile drone formations must be capable of high-maneuverability turns. For omnidirectional affine formations, the traversal direction is determined by the formation hierarchy configuration  $\mathcal{G}^i(\mathcal{V}^i, \mathcal{E}^i)$ ,  $i = 1, 2, \dots, r$ . To facilitate the formation's swift adaptation to any given environment  $\mathbf{E}$ , this problem can be modeled as follows:

$$\mathcal{G}^i(\mathcal{V}^i, \mathcal{E}^i) = F(j \mathbf{x}, j \hat{\mathbf{x}}, \mathbb{G}) \quad (4)$$

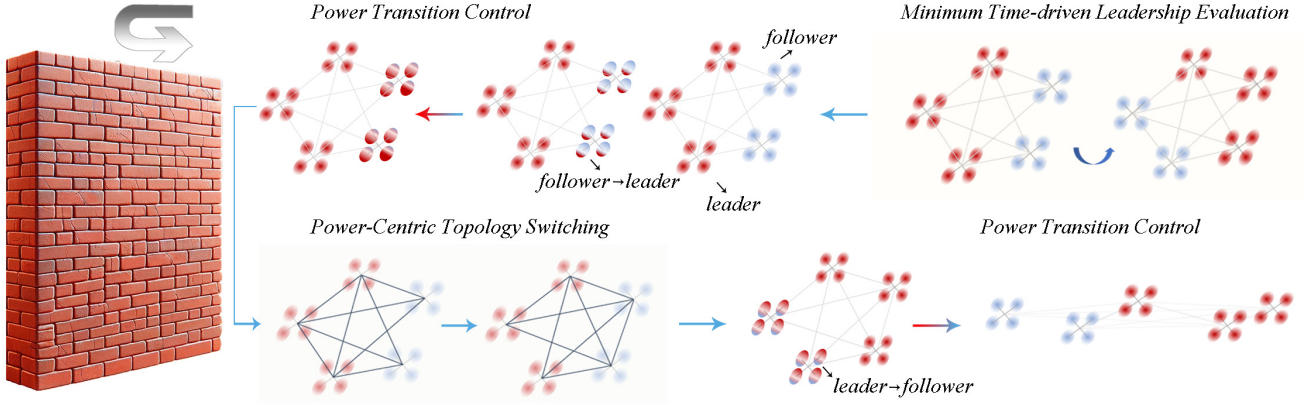


Fig. 1. The architecture of the proposed omnidirectional affine formation strategy. In formations eligible for hierarchical reorganizations, the initial step involves validating individual roles, as determined by a minimum time-driven leadership evaluation algorithm. As the formation nears the transition juncture, followers designated to assume leadership are seamlessly transitioned through implementing a power transition control algorithm. Upon arrival at the transition point, a strategic reorganization in the formation's topological structure is executed, utilizing a power-centric topology switching strategy. This reconfigured topological structure then serves as the basis for applying the power transition control strategy. This application is focused on the smooth devolution of authority from the leader transitioning to a follower role, thereby ensuring a fluid and uninterrupted transition within the hierarchical reorganization process of the formation.

where  $\mathbb{G} = \{\mathcal{G}^1(\mathcal{V}^1, \mathcal{E}^1), \dots, \mathcal{G}^r(\mathcal{V}^r, \mathcal{E}^r)\}$  is the feasible formation configuration set, the  ${}^j\mathbf{x}$  and  ${}^j\hat{\mathbf{x}}$  represent the current state and target state of drone  $j$ , respectively.

#### IV. OMNIDIRECTIONAL AFFINE FORMATION BASED ON HIERARCHICAL REORGANIZATIONS

This section comprehensively elaborates on the specific methods of omnidirectional affine formation, divided into three distinct parts, with the overall system framework depicted in Fig. 1. The figure illustrates the inherent connections between these different components. Firstly, we define the omnidirectional affine formation and analyze the necessary conditions for hierarchical reorganizations. On this basis, we establish a minimum time-driven leadership evaluation algorithm tailored for the flexibility and coordination of the swarm to facilitate role recognition among different robots. Given the challenges of synchronous role switching in actual systems, we first introduce a power transition control strategy for smooth power transition by designing a power handover function. To eliminate disturbances caused by other followers, a power-centric topology switching strategy is proposed to facilitate the smooth execution of hierarchical reorganizations.

##### A. Omnidirectional Affine Formation

**Definition 1. (Dynamic Affine Localizability)** For the changing graph configuration  $\mathcal{G}(\mathcal{V}(t), \mathcal{E}(t))$ , the position of followers  $\{\mathbf{r}_i\}_{i \in \mathcal{V}_f(t)}$  can be uniquely determined by the position of leaders  $\{\mathbf{r}_i\}_{i \in \mathcal{V}_l(t)}$ .

**Assumption 1. (Initial Formation for Dynamic Affine Localizability):** For the initial formation  $(\mathcal{G}^o, \mathbf{r}^o)$ , assume that  $\{\mathbf{r}_i^o\}_{i \in \mathcal{V}_l^o}$  affinely span  $\mathbf{R}^d$ .

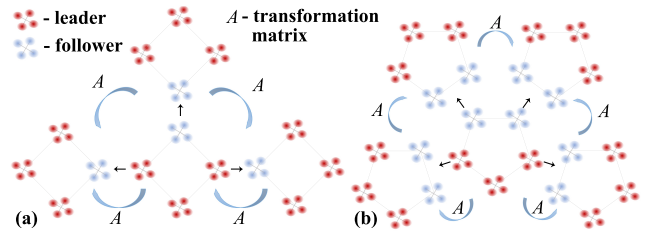


Fig. 2. Illustration of Initial Configuration for Omnidirectional Affine Formation. (a) Four drones formation. (b) Five drones formation.

**Theorem IV.1. (Hierarchical Reorganization for Dynamic Affine Localizability):** Under Assumption 1, the changing formation  $(\mathcal{G}^t, \mathbf{r}^t)$  is dynamically affine localizable if and only if  $\{\mathbf{r}_i^t\}_{i \in \mathcal{V}_l^t}$  affinely span  $\mathbf{R}^d$ .

*Proof.* (Sufficiency) According to the *Theorem 1* in [8], the formation  $(\mathcal{G}, \mathbf{r})$  is affinely localizable if and only if  $\{\mathbf{r}_i\}_{i \in \mathcal{V}_l}$  affinely span  $\mathbf{R}^d$ . For any formation  $(\mathcal{G}^{t_1}, \mathbf{r}^{t_1}) \in (\mathcal{G}^t, \mathbf{r}^t)$ ,  $(\mathcal{G}^{t_1}, \mathbf{r}^{t_1})$  is affinely localizable if  $\{\mathbf{r}_i\}_{i \in \mathcal{V}_l^{t_1}}$  affinely span  $\mathbf{R}^d$ . Then,  $(\mathcal{G}^t, \mathbf{r}^t)$  is dynamically affine localizable consequently.

(Necessity) For any formation  $(\mathcal{G}^{t_1}, \mathbf{r}^{t_1}) \in (\mathcal{G}^t, \mathbf{r}^t)$ ,  $(\mathcal{G}^{t_1}, \mathbf{r}^{t_1})$  cannot realize affine localizability if  $\{\mathbf{r}_i\}_{i \in \mathcal{V}_l^{t_1}}$  cannot affinely span  $\mathbf{R}^d$ . Then,  $(\mathcal{G}^t, \mathbf{r}^t)$  cannot satisfy dynamically affine localizability consequently.  $\square$

**Definition 2. (Omnidirectional Affine Formation)** For the changing formation  $(\mathcal{G}^t, \mathbf{r}^t)$ , any target configuration  $\mathbf{p}^*$  of current nominal configuration  $\mathbf{r}^t$  locates at the same affine image  $\mathcal{A}(\mathbf{r}^t)$ .

**Assumption 2. (Initial Configuration for Omnidirectional Affine Formation)** For any initial configuration  $\mathbf{r}^o$ , assume that  $C(n, n_l) \geq 1$  where  $C(n, n_l)$  represents the count of

viable combinations for hierarchical reorganization within  $\mathbf{r}^o$ .

**Theorem IV.2.** (Omnidirectional Affine Formable) Under Assumptions 1 and 2, the dynamic configuration  $\mathbf{p}$  is omnidirectional affine formable if and only if the initial configuration  $\mathbf{r}^o$  satisfies that  $\{\mathbf{r}^{o_j}\}_{j \in [1, C(n, n_i)]} \in \mathcal{A}(\mathbf{r}^o)$ .

*Proof.* (Sufficiency) if  $\{\mathbf{r}^{o_j}\}_{j \in [1, C(n, n_i)]} \in \mathcal{A}(\mathbf{r}^o)$ , there always exists  $(\mathbf{A}', b')$  satisfying

$$\mathbf{r}^{o_j} = (\mathbf{I}_n \otimes \mathbf{A}')\mathbf{r}^o + \mathbf{1}_n \otimes b' \quad (5)$$

Based on the property of affine transformation, the matrix  $\mathbf{A}$  is invertible [33], which means the inverse of  $\mathbf{I}_n \otimes \mathbf{A}'$  exists. Then,

$$\mathbf{r}^o = (\mathbf{I}_n \otimes \mathbf{A}'^{-1})\mathbf{r}^{o_j} - \mathbf{1}_n \otimes (\mathbf{A}'^{-1} \cdot b') \quad (6)$$

Assume that the configuration  $\mathbf{p} \in \mathcal{A}(\mathbf{r}^o)$  represents the pre-formation in the first leader switching, then there always exists  $(\mathbf{A}^m, b^m)$  satisfying

$$\mathbf{p} = (\mathbf{I}_n \otimes \mathbf{A}^m)\mathbf{r}^o + \mathbf{1}_n \otimes b^m \quad (7)$$

Substituting  $\mathbf{r}^o$  with  $(\mathbf{I}_n \otimes \mathbf{A}'^{-1})\mathbf{r}^{o_j} - \mathbf{1}_n \otimes (\mathbf{A}'^{-1} \cdot b')$ , then  $\mathbf{p}$  can be reformulated as

$$\mathbf{p} = (\mathbf{I}_n \otimes \mathbf{A}^m \mathbf{A}'^{-1})\mathbf{r}^{o_j} - \mathbf{1}_n \otimes (b^m - \mathbf{A}^m \mathbf{A}'^{-1} b') \quad (8)$$

Make  $\mathbf{A}^{m'} = \mathbf{A}^m \mathbf{A}'^{-1}$  and  $b^{m'} = b^m - \mathbf{A}^m \mathbf{A}'^{-1} b'$ , then

$$\mathbf{p}' = \mathbf{p} = (\mathbf{I}_n \otimes \mathbf{A}^{m'})\mathbf{r}^{o_j} + \mathbf{1}_n \otimes b^{m'} \quad (9)$$

where  $\mathbf{p}'$  represents the post-formation after switching leader. Since  $\mathbf{p}' \in \mathcal{A}(\mathbf{r}^{o_j})$  and  $\mathcal{A}(\mathbf{r}^o) = \mathcal{A}(\mathbf{r}^{o_j})$ , the dynamic formation  $(\mathcal{G}^t, \mathbf{r}^t)$  is affinely formable consequently.

(Necessity) Taking the first leader switching as an example, there always exists  $(\mathbf{A}^m, b^m)$  satisfying

$$\mathbf{p} = (\mathbf{I}_n \otimes \mathbf{A}^m)\mathbf{r}^o + \mathbf{1}_n \otimes b^m \quad (10)$$

where  $\mathbf{p} \in \mathcal{A}(\mathbf{r}^o)$  represents the pre-formation. Since  $\mathbf{p}' = \mathbf{M}\mathbf{p}$  where  $\mathbf{p}'$  and  $\mathbf{M}$  represent the post-formation and the transfer matrix, respectively, then

$$\mathbf{p}' = (\mathbf{I}_n \otimes \mathbf{A}')\mathbf{M}\mathbf{p} + \mathbf{1}_n \otimes b' \quad (11)$$

Substituting  $\mathbf{p}$  with  $\mathbf{r}^o$ , then  $\mathbf{p}'$  can be reconstructed as

$$\mathbf{p}' = (\mathbf{I}_n \otimes \mathbf{A}' \mathbf{A}^m)\mathbf{M}\mathbf{r}^o + \mathbf{1}_n \otimes (\mathbf{M}\mathbf{A}' b^m + b') \quad (12)$$

Since  $\mathbf{r}^{o_j} = \mathbf{M}\mathbf{r}^o$ , then

$$\mathbf{p}' = (\mathbf{I}_n \otimes \mathbf{A}^{m'})\mathbf{r}^{o_j} + \mathbf{1}_n \otimes b^{m'} \quad (13)$$

where  $\mathbf{A}^{m'} = (\mathbf{I}_n \otimes \mathbf{A}' \mathbf{A}^m)$  and  $b^{m'} = \mathbf{M}\mathbf{A}' b^m + b'$ . Then,  $\mathbf{p}' \in \mathcal{A}(\mathbf{r}^{o_j})$ . If  $\mathcal{A}(\mathbf{r}^o) \neq \mathcal{A}(\mathbf{r}^{o_j})$ ,  $\mathbf{p}' \notin \mathcal{A}(\mathbf{r}^{o_j})$ . The dynamic formation  $(\mathcal{G}^t, \mathbf{r}^t)$  cannot satisfy affine localizability consequently.  $\square$

Several omnidirectional affine formations are depicted in Fig.2. For a changing formation  $\mathcal{G}^t$  satisfying Theorem IV.1 and IV.2, we can identify a collection of viable formations from  $\{\mathbf{r}^{o_j}\}_{j \in [1, C(n, n_i)]} \in \mathcal{A}(\mathbf{r}^o)$  represented as  $\mathbb{G}$ .

In determining the optimal formation post-hierarchical reorganization, the leadership evaluation encompasses a twofold assessment: the overall flexibility of the formation and the maneuverability of each agent. Fig. 3 illustrates the minimum time-driven leadership evaluation algorithm process, providing a clear visual representation of the methodology applied to hierarchical reorganization. First, when the relevant formation collection  $\mathcal{G}^i$  is determined, the leadership evaluation index can be initially defined as:

$$\Theta \leftarrow \min_{i=1,2,\dots,r} (t_j^{\mathcal{G}^i}) \quad \mathcal{G}^i \in \mathbb{G} \quad (14)$$

where  $t_j^{\mathcal{G}^i}$  represents the required time for the formation collection  $\mathcal{G}^i$  from current location to target location. Specifically, the  $t_j^{\mathcal{G}^i}$  is expressed as the flight time required for the agent  $j$  from its current location  ${}^j\hat{\mathbf{x}}$  to reach its corresponding target location in  $\mathcal{G}^i$ , which is denoted as  ${}^j\hat{\mathbf{x}}^{\mathcal{G}^i}$ . In this paper, the  $\Phi(\cdot)$  representing the trajectory generation algorithm is applied to calculate  $t_j^{\mathcal{G}^i}$  and obtain the set of trajectory points  $\mathbb{P}^j$  of agent  $j$ , which is formulated as:

$$\begin{aligned} (t_j^{\mathcal{G}^i}, \mathbb{P}^j) &= \Phi({}^j\hat{\mathbf{x}}, {}^j\hat{\mathbf{x}}^{\mathcal{G}^i}) \\ \text{s.t. } \max({}^j\mathbf{x}^{(1)}) &\leq {}^j v^{max} \quad \min({}^j\mathbf{x}^{(1)}) \geq {}^j v^{min} \\ \max({}^j\mathbf{x}^{(2)}) &\leq {}^j a^{max} \quad \min({}^j\mathbf{x}^{(2)}) \geq {}^j a^{min} \end{aligned} \quad (15)$$

where  ${}^j v^{max}$  and  ${}^j v^{min}$  represent the maximum and minimum velocities for agent  $j$ , respectively. Meanwhile,  ${}^j a^{max}$  and  ${}^j a^{min}$  represent the maximum and minimum accelerations for agent  $j$ , respectively. To ensure the maneuverability of each agent while achieving synchronicity within the formation. For any agent  $j$ , the flight time is standardized to the maximum value of the individual planning time. Then, for the formation collection  $\mathbb{G}$ , the leadership evaluation index can be reformulated as:

$$\begin{aligned} (\Theta, \tau) &\leftarrow \min_{i=1,2,\dots,r} \left( \max_{k=1,2,\dots,n} (t_k^{\mathcal{G}^i}) \right) \\ \text{s.t. } \mathcal{G}^i &\in \mathbb{G} \end{aligned} \quad (16)$$

where  $\tau$  represents the actual planning time with the selected formation configuration  $\Theta$ .

### B. Power Transition Control Algorithm

In hierarchical formation, control under affine transformations typically manifests as leaders and followers employing distinct strategies. We first consider the control of the leader. Based on the formation configuration  $\Theta$  and the planned time  $\tau$  derived from Eq.(16), the set of discrete point motion states for each agent  $i$  at each moment can be expressed as:

$$\mathbb{P}^i = \Phi({}^i\hat{\mathbf{x}}, {}^i\hat{\mathbf{x}}^\Theta, \tau) \quad (17)$$

Therefore, for the leader  $i$  at time  $T(k+1)$ , the target position is  $\hat{\mathbf{p}}_i^{T(k+1)} \in \mathbb{P}^i$ . For the leader, it is only necessary to track the state of the target point in real-time at  $T(k+1)$ .

Secondly, the control strategy of follower  $i$  at time  $T(k+1)$

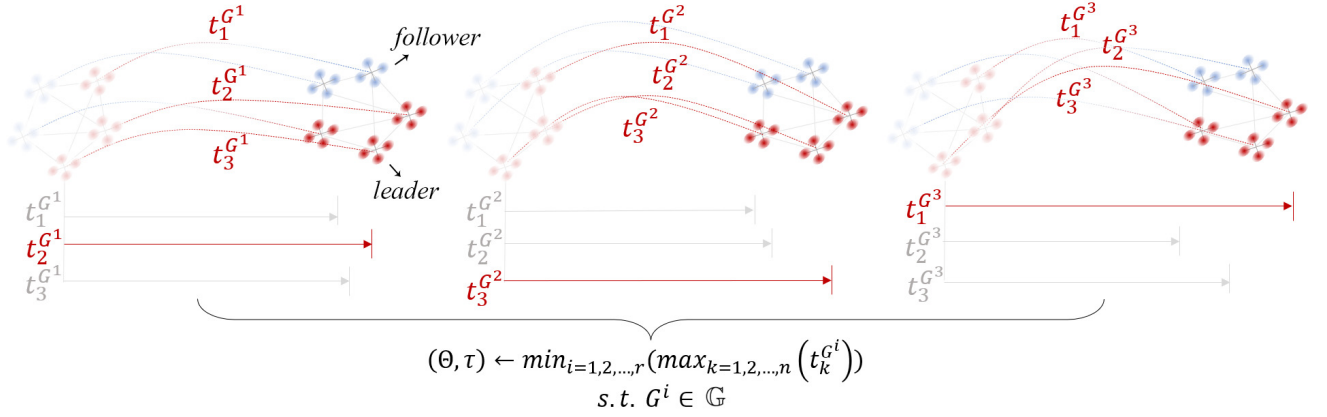


Fig. 3. Process of leadership evaluation.

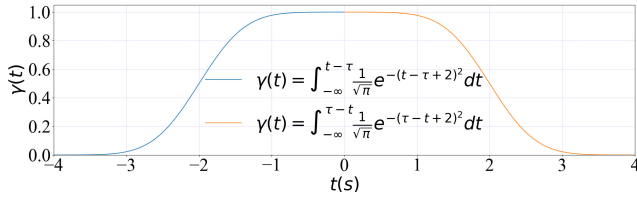


Fig. 4. The power transfer function.

1) is described as:

$$\mathbf{p}_i^{T(k+1)} = \mathbf{p}_i^{T(k)} - \frac{\sum_{j \in N_i} \omega_i^j (\mathbf{p}_i^{T(k)} - \mathbf{p}_j^{T(k)} - \mathbf{v}_j^{T(k)})}{\sum_{j \in N_i} \omega_i^j} \delta T(k+1)$$

$$\delta T(k+1) = T(k+1) - T(k) \quad (18)$$

This strategy achieves the control of the follower, maintaining the affine formation while following the leader.

Unlike the control strategy, where the leader does not switch, hierarchical reorganization reflects the power transfer. It is evident that Eq.(17) represents the pinnacle of individual power. Conversely, Eq.(18) signifies the complete dissipation of individual power. To address this characteristic, we design a power transfer function to demonstrate the features of different power transfer processes. Since the transition from follower to leader signifies an expansion of individual rights, and the transition from leader to follower represents a reduction of individual power, the power transfer function is designed as follows:

$$\gamma(t) = \begin{cases} \gamma_f, & 0 \leq \gamma_f \leq 1, & \text{follower} \rightarrow \text{follower} \\ \int_{-\infty}^{t-\tau} \frac{1}{\sqrt{\pi}} e^{-(t-\tau+2)^2} dt, & \text{follower} \rightarrow \text{leader} \\ \int_{-\infty}^{\tau-t} \frac{1}{\sqrt{\pi}} e^{-(\tau-t+2)^2} dt, & \text{leader} \rightarrow \text{follower} \\ 1, & \text{leader} \rightarrow \text{leader} \end{cases} \quad (19)$$

Where  $t \in [0, \tau]$ . The power transfer function is shown in Fig. 4. Consequently, during the hierarchical reorganization process, the control function can be designed as:

$$d\mathbf{p}_i^{T(k+1)} = (1 - \gamma(t))\mathbf{p}_i^{T(k+1)} + \gamma(t)\hat{\mathbf{p}}_i^{T(k+1)} \quad (20)$$

**Assumption 3.** (Target Trajectory for Followers) For any follower  $i$ , assume that  $\mathbf{p}_i^{T(k+1)}$  is on the target trajectory.

**Theorem IV.3.** (Convergence of Power Transition Control) Under the Assumption 3, the convergence rate of Eq. (20) is faster than  $e^t$ .

*Proof.* According to the definition of  $\hat{\mathbf{p}}_i^{T(k+1)}$ , the control error can be expressed as:

$$d\delta\mathbf{p}_i^{T(k+1)} = \hat{\mathbf{p}}_i^{T(k+1)} - [(1 - \gamma(t))\mathbf{p}_i^{T(k+1)} + \gamma(t)\hat{\mathbf{p}}_i^{T(k+1)}]$$

$$= (1 - \gamma(t))(\hat{\mathbf{p}}_i^{T(k+1)} - \mathbf{p}_i^{T(k+1)}) \quad (21)$$

Denote  $\delta\mathbf{p}_i^{T(k+1)} = \hat{\mathbf{p}}_i^{T(k+1)} - \mathbf{p}_i^{T(k+1)}$ , then the control error is reformulated as:

$$d\delta\mathbf{p}_i^{T(k+1)} = (1 - \gamma(t))(\delta\mathbf{p}_i^{T(k+1)}) \quad (22)$$

Substitute  $\mathbf{p}_i^{T(k+1)}$  with Eq.(18), we can obtain that

$$\delta\mathbf{p}_i^{T(k+1)} = \hat{\mathbf{p}}_i^{T(k+1)} - \mathbf{p}_i^{T(k+1)} = \hat{\mathbf{p}}_i^{T(k+1)} - \mathbf{p}_i^{T(k)} + \frac{1}{\sum_{j \in N_i} \omega_i^j} (\sum_{j \in N_i} \omega_i^j (\mathbf{p}_i^{T(k)} - \mathbf{p}_j^{T(k)} - \mathbf{v}_j^{T(k)})) \delta T(k+1) \quad (23)$$

Simplify the Eq.(23), we can obtain that:

$$\sum_{j \in N_i} \omega_i^j (\mathbf{p}_i^{T(k)} - \mathbf{p}_j^{T(k)}) + \sum_{j \in N_i} \omega_i^j (\mathbf{v}_i^{T(k)} - \mathbf{v}_j^{T(k)}) = 0 \quad (24)$$

According to Section III-B, the local matrix-vector form in Eq.(24) is

$$\sum_{j \in N_i} \omega_i^j (\mathbf{p}_i^{T(k)} - \mathbf{p}_j^{T(k)}) = \bar{\Omega}_{ff} \mathbf{p}_f + \bar{\Omega}_{fl} \mathbf{p}_l^* = \bar{\Omega}_{ff} \delta \mathbf{p}_f$$

$$\sum_{j \in N_i} \omega_i^j (\mathbf{v}_i^{T(k)} - \mathbf{v}_j^{T(k)}) = \bar{\Omega}_{ff} \mathbf{v}_f + \bar{\Omega}_{fl} \mathbf{v}_l^* = \bar{\Omega}_{ff} \delta \mathbf{v}_f \quad (25)$$

Then, the matrix-vector of Eq.(24) can be formulated as:

$$\bar{\Omega}_{ff} \delta \mathbf{p}_f + \bar{\Omega}_{ff} \delta \mathbf{v}_f = \mathbf{0} \quad (26)$$

As  $\delta \mathbf{v}_f = \dot{\delta} \mathbf{p}_f$  and  $\bar{\Omega}_{ff}$  is positive definite, we have  $\dot{\delta} \mathbf{p} = \delta \mathbf{p}$ , which implies  $\delta \mathbf{p}$  converges to zero globally

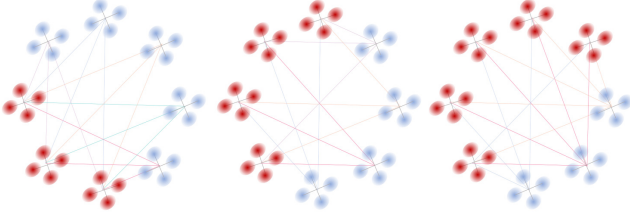


Fig. 5. Illustration for power-centric topology switching.

and exponentially fast.

According to the definition of  $\gamma(t)$ ,  $\gamma(t) \leq 1$  always holds, which means  $1 - \gamma(t) \leq 1$  always satisfies. From Eq.(22), the control error satisfies:

$$d\delta\mathbf{p}_i^{T(k+1)} = (1 - \gamma(t))\delta\mathbf{p}_i^{T(k+1)} \leq \delta\mathbf{p}_i^{T(k+1)} \quad (27)$$

which implies that the proposed control function converges globally and at a faster rate than  $e^t$ .  $\square$

### C. Power-Centric Topology Switching

The control strategy outlined in Section IV-B reveals a temporal difference in the expected position updates across various hierarchical formation levels. The follower's position, inherently dependent on topological relationships, exhibits a coupling effect between the formation's inherent topological structures and the temporal difference, affecting the control accuracy. Considering the dynamic change of individual roles within the hierarchical reorganization, invariant topological connections can compromise control accuracy. In response, this section delves into a power-centric topological switching approach designed to mitigate the influence of topological connections in tandem with the hierarchical reorganization process.

**Lemma IV.1.** (Generic Graph Configuration [33]) For the dynamic formation  $\mathcal{G}(\mathcal{V}(t), \mathcal{E}(t))$ , if and only if  $\mathcal{G}(\mathcal{V}(t), \mathcal{E}(t))$  is  $(d + 1) -$  rooted, the stress matrix  $\Omega$  is semi-positive and  $\text{rank}(\Omega) = n - d - 1$ .

**Assumption 4.** For the dynamic formation  $\mathcal{G}(\mathcal{V}(t), \mathcal{E}(t))$ ,  $\mathcal{G}(\mathcal{V}(t), \mathcal{E}(t))$  is  $(d + 1) -$  rooted.

**Theorem IV.4.** (Topology Configuration for Omnidirectional Affine Localizability) Under the Assumption 4, for the dynamic formation  $\mathcal{G}(\mathcal{V}(t), \mathcal{E}(t))$ , when each follower is topologically connected only to leaders,  $\mathcal{G}(\mathcal{V}(t), \mathcal{E}(t))$  can achieve omnidirectional affine localizability.

*Proof.* When  $\mathcal{G}(\mathcal{V}(t), \mathcal{E}(t))$  is  $(d + 1) -$  rooted, there exists at least  $(d + 1) -$  neighbor for each follower. As each follower is topologically connected only to leaders, each follower will be topologically connected to at least  $(d + 1)$  leaders. Under this circumstance, the adjacent matrix  $D$  can be reconstructed as  $D = \begin{bmatrix} D_{ll} & D_{lf} \\ \mathbf{0} & D_{ff} \end{bmatrix}$ . Denote the total number of edges between the follower  $i$  and leaders as  $n_{ef}^i$ . As there is no topological connection

between followers, then  $D_{ff}$  can be expressed as:

$$D_{ff} = \begin{bmatrix} -\mathbf{1} \in \mathbf{R}^{1 \times n_{ef}^1} & \mathbf{0} \in \mathbf{R}^{1 \times n_{ef}^2} & \dots & \mathbf{0} \in \mathbf{R}^{1 \times n_{ef}^{n_f}} \\ \mathbf{0} \in \mathbf{R}^{1 \times n_{ef}^1} & -\mathbf{1} \in \mathbf{R}^{1 \times n_{ef}^2} & \dots & \mathbf{0} \in \mathbf{R}^{1 \times n_{ef}^{n_f}} \\ \dots & \dots & \dots & \dots \\ \mathbf{0} \in \mathbf{R}^{1 \times n_{ef}^1} & \mathbf{0} \in \mathbf{R}^{1 \times n_{ef}^2} & \dots & -\mathbf{1} \in \mathbf{R}^{1 \times n_{ef}^{n_f}} \end{bmatrix}$$

where  $\mathbf{1}$  and  $\mathbf{0}$  implies all-1 and all-0 vector, respectively. As  $\Omega = D \text{diag}(\omega) D^T$ , then,

$$\omega_{ef} = \{\omega_1^1, \dots, \omega_1^{n_{ef}^1}, \dots, \omega_{n_f}^1, \dots, \omega_{n_f}^{n_{ef}^{n_f}}\}. \quad (28)$$

The stress block  $\Omega_{ff}$  can be constructed as:

$$\Omega_{ff} = D_{ff} \text{diag}(\omega_{ef}) D_{ff}^T = \bigoplus_{i=1}^{n_f} \sum_{j=1}^{n_{ef}^i} \omega_i^j \quad (29)$$

According to the stress equilibrium condition, for each follower  $i$ ,  $\sum_{j=1}^{n_{ef}^i} \omega_i^j (\mathbf{r}_i - \mathbf{r}_j) = 0$ , where  $\mathbf{r}_i$  and  $\mathbf{r}_j$  represent the initial configuration of follower and leader, respectively. With this prerequisite, we can obtain that  $\sum_{j=1}^{n_{ef}^i} \omega_i^j \neq 0$ , which is proved in Proposition 1. Under this condition,

$$\det(\Omega_{ff}) = \left| \prod_{i=1}^{n_f} \left( \sum_{j=1}^{n_{ef}^i} \omega_i^j \right) \right| > 0 \quad (30)$$

Based on the characteristics of the matrix  $\det$ ,  $\Omega_{ff}$  is nonsingular, which means  $\mathcal{G}(\mathcal{V}(t), \mathcal{E}(t))$  can achieve affine localizability.  $\square$

**Proposition 1.** (Stress characteristics for followers) For a dynamic formation  $\mathcal{G}(\mathcal{V}(t), \mathcal{E}(t))$  that satisfies Assumption 4, when each follower is topologically connected only to the leader,  $\sum_{j=1}^{n_{ef}^i} \omega_i^j \neq 0$ , where  $n_{ef}^i$  denotes the total number of edges between follower  $i$  and leaders.

*Proof.* (contradiction) For follower  $i$ , assume  $\sum_{j=1}^{n_{ef}^i} \omega_i^j = 0$ , then  $\omega_i^{n_{ef}^i} = -\sum_{j=1}^{n_{ef}^i-1} \omega_i^j$ . According to the stress equilibrium condition, for each follower  $i$ ,  $\sum_{j=1}^{n_{ef}^i} \omega_i^j (\mathbf{r}_i - \mathbf{r}_j) = 0$ , where  $\mathbf{r}_i$  and  $\mathbf{r}_j$  represent the initial configuration of follower and leader, respectively. From this, we can obtain that:

$$\sum_{j=1}^{n_{ef}^i-1} \omega_i^j (\mathbf{r}_i - \mathbf{r}_j) - \sum_{j=1}^{n_{ef}^i-1} \omega_i^j (\mathbf{r}_i - \mathbf{r}_{n_{ef}^i}) = 0 \quad (31)$$

Simplification of the above equation yields that:

$$\sum_{j=1}^{n_{ef}^i-1} \omega_i^j \mathbf{r}_j - \sum_{j=1}^{n_{ef}^i-1} \omega_i^j \mathbf{r}_{n_{ef}^i} = 0 \quad (32)$$

As the topological connectivity exists only between follower  $i$  and leaders, then,  $n_{ef}^i \leq n_i$ . Complementing the non-existent  $\mathbf{r}_j$  in Eq.(32) with 0, then Eq.(32) can be

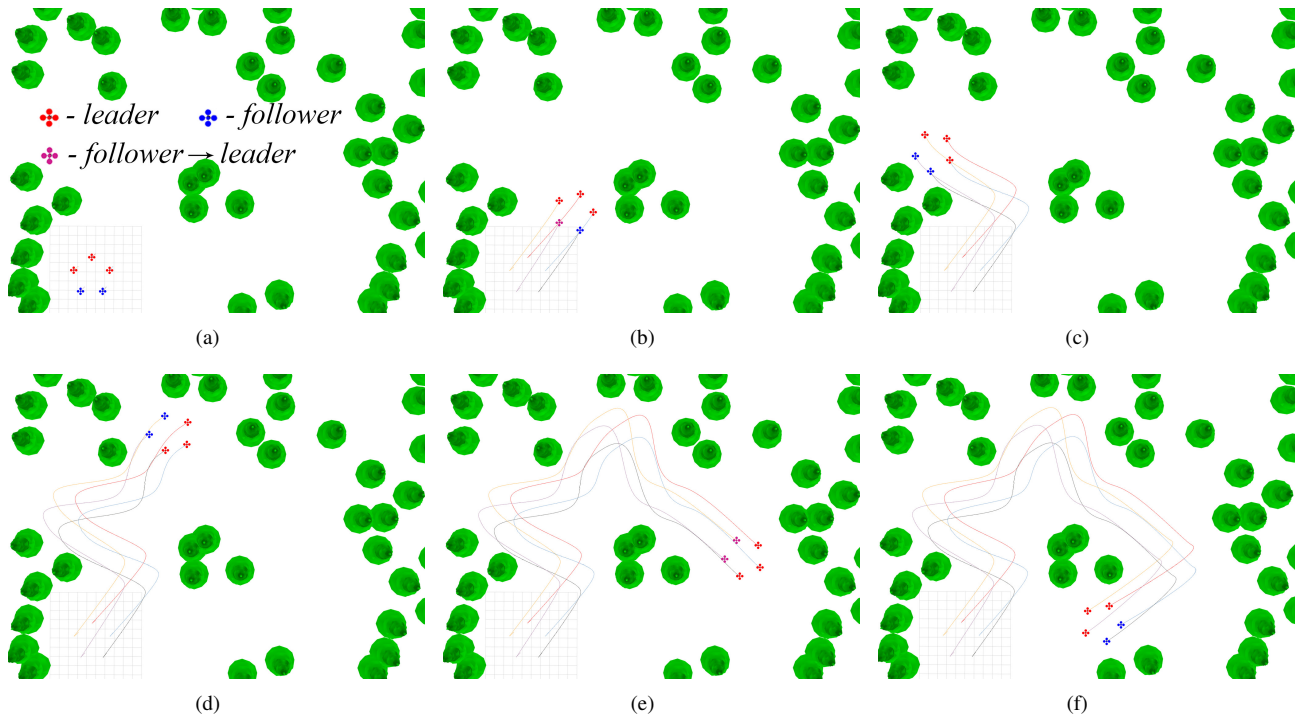


Fig. 6. Simulation process.

reconstructed as:

$$\sum_{j=1}^{n_l-1} \omega_i^j \mathbf{r}_j - \sum_{j=1}^{n_l-1} \omega_i^j \mathbf{r}_{n_l} = 0 \quad (33)$$

Denote  $\bar{\mathbf{r}} = \begin{bmatrix} \mathbf{r}_1^T & \mathbf{r}_2^T & \dots & \mathbf{r}_{n_l}^T \\ \mathbf{1} & \mathbf{1} & \dots & \mathbf{1} \end{bmatrix}^T$ , then  $\bar{\mathbf{r}}^T \boldsymbol{\omega} = 0$ . However, according to the Lemma 1 in [8],  $\text{rank}(\bar{\mathbf{r}}) = d + 1$ , which implies  $\bar{\mathbf{r}}^T$  is of row-full rank. Then, from the properties of vector spaces, only zero vectors exist in the zero space of  $\bar{\mathbf{r}}^T$ . According to the definition of  $\boldsymbol{\omega}$  in Eq.(2),  $\sum_{j=1}^{n_{ef}} |\omega_i^j| > 0$ , which contradicts the above inference obviously.  $\square$

According to Theorem IV.4, when the hierarchical reorganization is completed through Section IV-A, the topological connection structure in the current configuration is reset, such that each follower establishes a topological connection only with leaders. An example of topological switch is shown in Fig. 5.

## V. EXPERIMENTAL VERIFICATION

### A. Simulation

The simulation test is carried out in the robot operating system (ROS) + Gazebo + PX4. Fig. 6 shows the formation's overall movement process and trajectory. Five target points are set up during the simulation, and the formation performs a total of 5 hierarchical reorganizations.

Table I illustrates the impact of hierarchical reorganizations on the different drone path lengths. When employing the formation strategies, Drone 2 exhibits the longest

TABLE I  
COMPARISON OF DIFFERENT DRONES' PATH LENGTH WITH OR WITHOUT HIERARCHICAL REORGANIZATIONS

Path Length(m)	Drone 0	Drone 1	Drone 2	Drone 3	Drone 4
With hierarchical reorganization	82.38	84.86	<b>85.33</b>	82.73	<b>81.22</b>
W/O hierarchical reorganization [8]	88.95	<b>90.30</b>	80.38	<b>72.29</b>	79.56

TABLE II  
COMPARISON OF DIFFERENT DRONES' VELOCITY WITH OR WITHOUT HIERARCHICAL REORGANIZATIONS

Velocity(m/s)	Drone 0	Drone 1	Drone 2	Drone 3	Drone 4
With hierarchical reorganization	2.12	2.18	<b>2.20</b>	2.12	<b>2.07</b>
W/O hierarchical reorganization [8]	2.39	<b>2.42</b>	2.14	<b>1.94</b>	2.14

motion path, measuring 85.33m, while Drone 4 covers the shortest distance at 81.22m, resulting in a difference of 4.11m. Conversely, without hierarchical reorganizations, Drone 1 records the longest motion path within the formation at 90.30m, while Drone 3 covers the shortest distance at 72.79m, yielding a substantial difference of 18.01m. This signifies that the omnidirectional affine formation strategies can effectively equalize the motion distances of drones, thereby significantly enhancing both the coordination within the formation and the formation's overall endurance.

Table II presents the influence of hierarchical reorganizations on the average motion speeds of different drones. When employing the omnidirectional affine formation strategy, Drone 2 achieves the highest motion speed, recording a speed of 2.20m/s, while Drone 4 exhibits the slowest





Fig. 7. Environment setup.

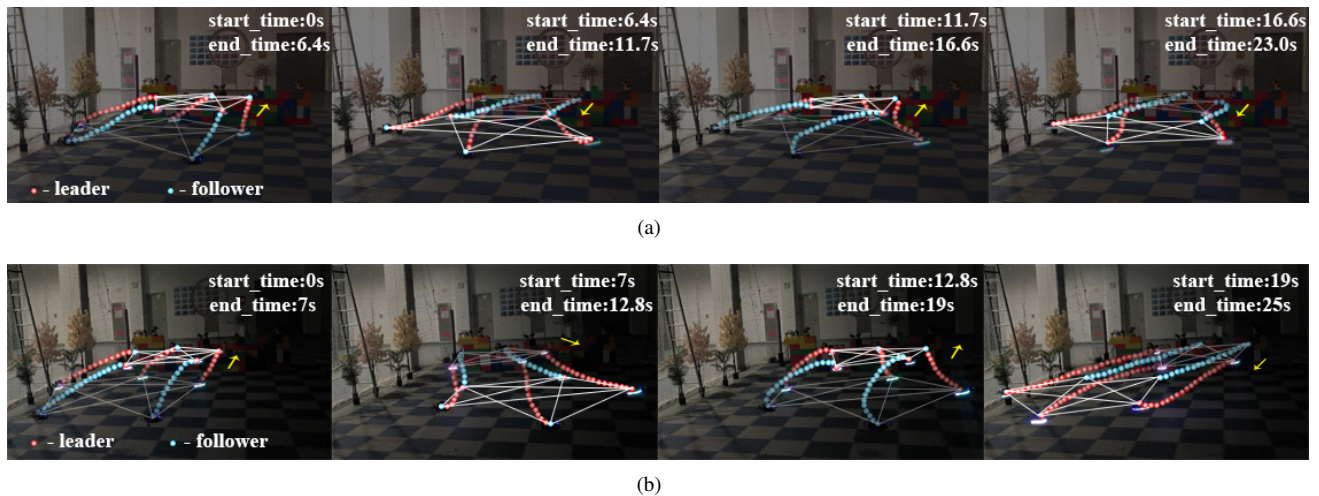


Fig. 8. The experimental process of formation flight with patterns '1' and '8'.

motion speed at  $2.07m/s$ , resulting in a difference of  $0.13m/s$ . In contrast, without the hierarchical reorganizations, Drone 1 attains the highest motion speed within the cluster at  $2.42m/s$ , while Drone 3 moves at the slowest speed of  $1.94m/s$ , resulting in a more substantial difference of  $0.48m/s$ . Furthermore, the overall motion durations for both approaches are  $38.93s$  and  $37.31s$ , respectively. This indicates that, with similar overall motion durations, the omnidirectional affine formation strategy significantly reduces the average speed disparities among individual entities, allowing the swarm to maintain similar motion speeds. Consequently, this enhances both the in-team coordination and flexibility of the formation.

### B. Experimental Setup

To verify the performance of the proposed algorithm, we conduct several indoor experiments, as shown in Fig. 7. Specifically, Fig. 7(a) depicts a scenario set within an obstacle-free dark environment, where five drones execute formation flights in the '1' and '8' patterns. Fig. 7(b) and Fig. 7(c) present environments featuring a hoop obstacle and a natural obstacle, respectively. In Fig. 7(b), the quintet of drones performs a coordinated obstacle avoidance flight through the hoop, whereas in Fig. 7(c), they engage in formation flights with free transformations

TABLE III  
 THE AVERAGE VELOCITY, PATH LENGTH AND TIMES OF SERVING AS LEADERS FOR DIFFERENT DRONE IN EXP. 1 AND EXP. 2

	Drone 0	Drone 1	Drone 2	Drone 3	Drone 4
	${}^0\bar{v}(m/s)$	${}^1\bar{v}(m/s)$	${}^2\bar{v}(m/s)$	${}^3\bar{v}(m/s)$	${}^4\bar{v}(m/s)$
	0.62	0.63	0.59	0.60	0.60
Exp. 1	${}^0path(m)$	${}^1path(m)$	${}^2path(m)$	${}^3path(m)$	${}^4path(m)$
	14.59	14.73	13.34	14.38	14.73
	${}^0Times$	${}^1Times$	${}^2Times$	${}^3Times$	${}^4Times$
	2/3	2/3	3/3	2/3	3/3
	${}^0\bar{v}(m/s)$	${}^1\bar{v}(m/s)$	${}^2\bar{v}(m/s)$	${}^3\bar{v}(m/s)$	${}^4\bar{v}(m/s)$
	0.62	0.59	0.56	0.59	0.62
Exp. 2	${}^0path(m)$	${}^1path(m)$	${}^2path(m)$	${}^3path(m)$	${}^4path(m)$
	15.70	15.09	14.20	15.26	15.77
	${}^0Times$	${}^1Times$	${}^2Times$	${}^3Times$	${}^4Times$
	3/3	2/3	3/3	3/3	2/3

within the natural obstacle environment. The dimensions (length $\times$ width $\times$ height) of each drone are  $23cm \times 23cm \times 14cm$ . The IMU is embedded in each drone's flight control hardware, referred to as Pixhawk<sup>®</sup>. Moreover, the NOKOV<sup>®</sup> motion capture system provides the global position measurements, and an UP Board 4000<sup>®</sup> computing board running ROS is adopted as the onboard computer. A small TP-LINK<sup>®</sup> router model TL-WDR5650 is mounted on each drone to facilitate communication among multiple

TABLE IV

THE COST TIME FOR HIERARCHICAL REORGANIZATION OF DIFFERENT DRONE IN EXP. 1 AND EXP. 2

	Drone 0	Drone 1	Drone 2	Drone 3	Drone 4
Exp. 1	${}^0_1t(s)$	${}^1_1t(s)$	${}^2_1t(s)$	${}^3_1t(s)$	${}^4_1t(s)$
	0.037	0.038	0.039	0.038	0.037
	${}^0_2t(s)$	${}^1_2t(s)$	${}^2_2t(s)$	${}^3_2t(s)$	${}^4_2t(s)$
	0.039	0.037	0.040	0.033	0.038
Exp. 2	${}^0_3t(s)$	${}^1_3t(s)$	${}^2_3t(s)$	${}^3_3t(s)$	${}^4_3t(s)$
	-	-	0.040	-	0.036
	${}^0_1t(s)$	${}^1_1t(s)$	${}^2_1t(s)$	${}^3_1t(s)$	${}^4_1t(s)$
	0.040	0.038	0.039	0.040	0.037
Exp. 2	${}^0_2t(s)$	${}^1_2t(s)$	${}^2_2t(s)$	${}^3_2t(s)$	${}^4_2t(s)$
	0.037	0.037	<b>0.047</b>	0.043	-
	${}^0_3t(s)$	${}^1_3t(s)$	${}^2_3t(s)$	${}^3_3t(s)$	${}^4_3t(s)$
	0.038	-	0.037	0.038	-

TABLE V

THE TRACKING ERROR FOR DIFFERENT DRONE IN EXP. 1 AND EXP. 2

	Drone 0	Drone 1	Drone 2	Drone 3	Drone 4
Exp. 1	${}^0e_x(m)$	${}^1e_x(m)$	${}^2e_x(m)$	${}^3e_x(m)$	${}^4e_x(m)$
	0.003	0.004	-0.045	-0.063	-0.038
	${}^0e_y(m)$	${}^1e_y(m)$	${}^2e_y(m)$	${}^3e_y(m)$	${}^4e_y(m)$
	-0.071	0.051	0.107	0.003	-0.012
Exp. 2	${}^0e_x(m)$	${}^1e_x(m)$	${}^2e_x(m)$	${}^3e_x(m)$	${}^4e_x(m)$
	0.005	0.009	-0.022	-0.027	-0.014
	${}^0e_y(m)$	${}^1e_y(m)$	${}^2e_y(m)$	${}^3e_y(m)$	${}^4e_y(m)$
	-0.051	0.036	0.044	-0.001	0.027

drones. Each drone is equipped with a light strip, controlled via GPIO on the UP Board 4000<sup>®</sup> computing board. This setup allows for visualizing the hierarchical reorganization process within the swarm. When a drone's light strip is illuminated, it indicates that the drone is the current leader of the formation.

### C. Results Analysis

The formation flight trajectories during two instances of hierarchical reorganizations, referred to as Exp. 1 and Exp. 2, are depicted in Fig. 8(a) and 8(b), respectively. Five drones are initially arranged in a regular pentagon with a side length of  $1.2m$ . Besides, the white connecting lines between each two drones illustrate the current topology of the formation, and the four sub-figures in Fig. 8(a) and 8(b) record the flight trajectory points and topological connection structures during the intervals between two hierarchical reorganizations. In Exp. 1, the formation of hierarchical reorganizations at four nodes when  $t = 0s, 6.4s, 11.7s, 16.6s, 23s$ . Similarly, in Exp. 2, the formation also experiences four hierarchical reorganizations, occurring at  $t = 0s, 7s, 12.8s, 19s, 25s$ .

Table III compares the average flying velocity  ${}^i\bar{v}$ , path length  ${}^i\text{path}$  and the number of times each drone served as the leader  ${}^i\text{Times}$  in Exp. 1 and 2. These results further validate the outcomes of simulation experiments. During the hierarchical reorganization process, the average

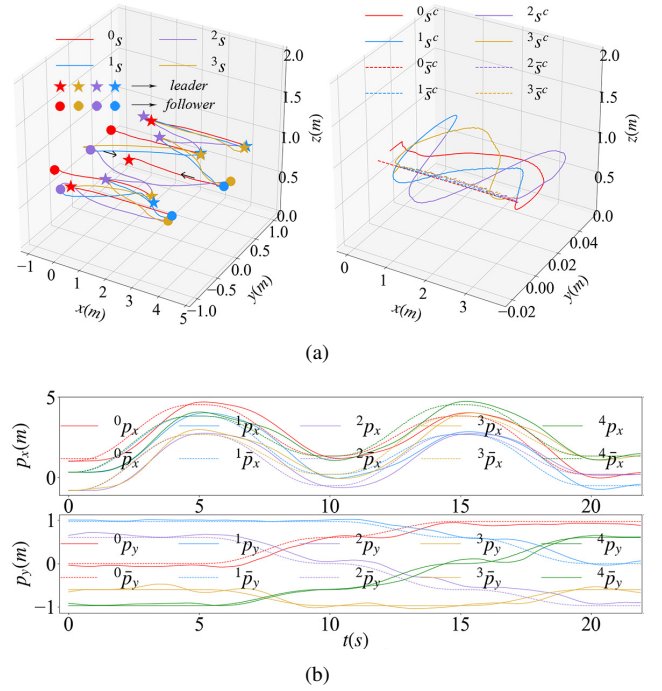


Fig. 9. The trajectory and track error of formation with patterns '1'.

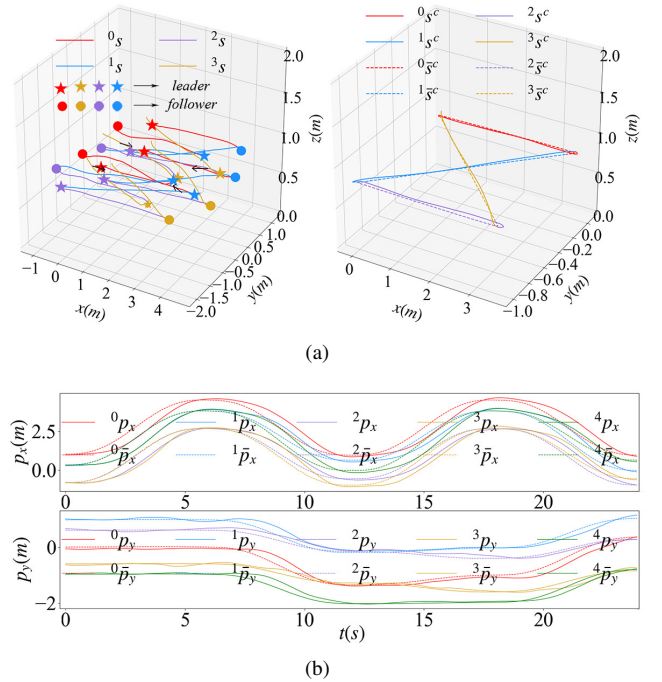


Fig. 10. The trajectory and track error of formation with patterns '8'.

velocities and path lengths among the drones are relatively similar, suggesting that the omnidirectional affine formation strategy enhances the in-team coordination of the swarm. The fact that  ${}^i\text{Times}$  is non-zero for all drones signifies that each one has acted as the leader at some point, implying that the current leadership evaluation algorithm demonstrates agile responsiveness to collective behaviors



Fig. 11. Hoop-traversing experiment.

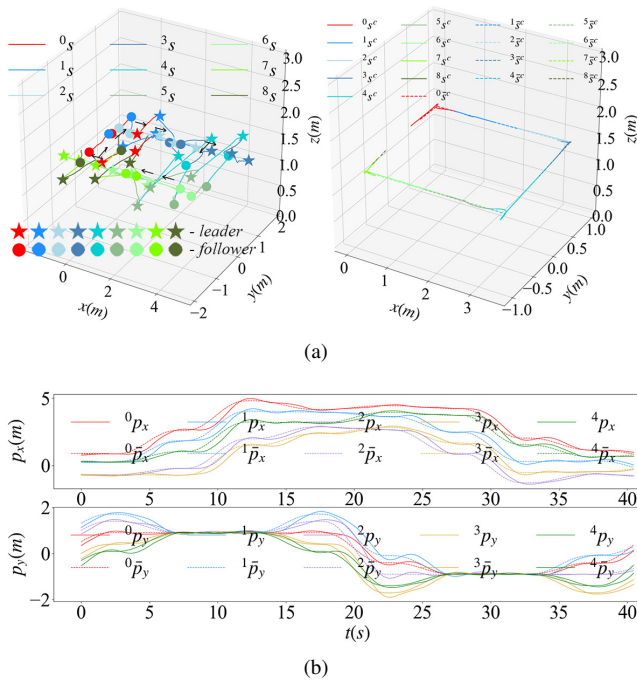


Fig. 12. The trajectory and track error of Exp. 3.

such as turning and U-turns. To calculate the cost time during hierarchical reorganizations, the role of each drone at every moment is recorded using *rosbag* at a frequency of 100Hz. By computing the interpolation between the moments before and after each drone's role transition, Table IV records the cost time for each drone during hierarchical reorganizations. Data analysis elucidates that the mean durations in Exp. 1 and Exp. 2 are 0.037s and 0.039s, respectively, marginally surpassing the operational control frequency of 30Hz. Notably, the maximum time is 0.047s, which implies that the formation can achieve swift hierarchical reorganization and smooth power transition.

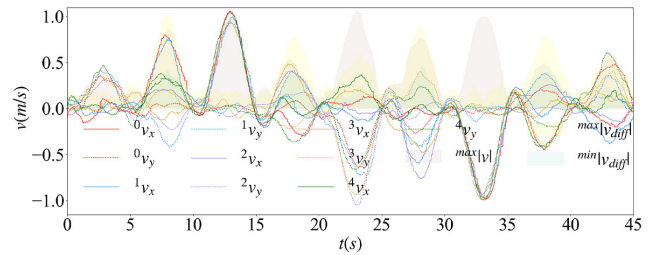


Fig. 13. The velocity curve of the formation in Exp. 3

Considering the transitions during hierarchical reorganizations, the actual trajectories and formation center tracking errors for Exp. 1 and 2 are illustrated in Fig. 9(a) and 10(a), respectively. Since a motion capture system is used for positioning during the experimental process, the impact of state estimation accuracy on the actual control effect is disregarded here. As shown in Fig. 9(a) and 10(a), the formation tracking error gradually decreases as it approaches the leader-switching points. Since the tracking performance of individual drones influences the center tracking error, combining this with the distribution patterns of individual drone velocity curves, it can be noted that the center tracking error decreases with a reduction in velocity. Besides, Table V records the tracking errors of different drones in Exp. 1 and 2, and the results show that the tracking errors among different drones are relatively similar. Fig. 9(b) and 10(b) present the expected and actual position curves for the  $x$  and  $y$  directions of different drones to investigate the distribution pattern of tracking errors. As depicted in Fig. 9(b) and 10(b), the actual position curves consistently lag behind the expected value curves, reflecting the latency inherent in the actual control system.

The hierarchical reorganization mechanism, combined with the affine formation crossing the hoop experiment, is illustrated in Fig 11, referred to as Exp. 3. In Exp.



Fig. 14. Dense formation transform experiment.

 TABLE VI  
 THE TRACKING ERROR FOR DIFFERENT DRONES AND FORMATION  
 TRANSFORM MATR IN EXP. 3

	Drone 0	Drone 1	Drone 2	Drone 3	Drone 4
	${}^0e_x(m)$	${}^1e_x(m)$	${}^2e_x(m)$	${}^3e_x(m)$	${}^4e_x(m)$
	-0.005	0.008	-0.015	-0.009	-0.007
	${}^0e_y(m)$	${}^1e_y(m)$	${}^2e_y(m)$	${}^3e_y(m)$	${}^4e_y(m)$
Exp. 3	0.005	0.016	0.023	0.017	0.004
	Transform Matrix				
	$\begin{bmatrix} 1 & 0 \\ 0 & 1 \end{bmatrix} \rightarrow \begin{bmatrix} 2 & 0 \\ 0.5 & 0 \end{bmatrix} \rightarrow \begin{bmatrix} 1 & 0 \\ 0 & 1 \end{bmatrix} \rightarrow \begin{bmatrix} 2 & 0 \\ 0.5 & 0 \end{bmatrix} \rightarrow \begin{bmatrix} 1 & 0 \\ 0 & 1 \end{bmatrix}$				

 TABLE VII  
 THE HIERARCHICAL REORGANIZATION SCENARIO AND FORMATION  
 TRANSFORM MATRIX IN EXP. 4

Leader Switching							
x	o	x	x	o	x	o	x
Transform Matrix							
$\begin{bmatrix} 1 & 0 \\ 0 & 1 \end{bmatrix} \rightarrow \begin{bmatrix} 0.8 & 0 \\ 0 & 0.8 \end{bmatrix} \rightarrow \begin{bmatrix} 2 & 0 \\ 0.5 & 0 \end{bmatrix} \rightarrow \begin{bmatrix} 1 & 0 \\ 0 & 1 \end{bmatrix} \rightarrow \begin{bmatrix} 1 & 0 \\ 0 & 1 \end{bmatrix}$							
$\rightarrow \begin{bmatrix} 0.8 & 0 \\ 0 & 0.8 \end{bmatrix} \rightarrow \begin{bmatrix} 2 & 0 \\ 0.5 & 0 \end{bmatrix} \rightarrow \begin{bmatrix} 0.8 & 0 \\ 0 & 0.8 \end{bmatrix} \rightarrow \begin{bmatrix} 1 & 0 \\ 0 & 1 \end{bmatrix}$							

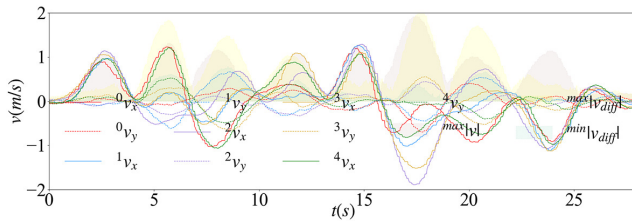


Fig. 15. The velocity curve of the formation in Exp. 4.

3, five drones are initially arranged in a regular pentagon with side lengths of  $1m$ . The formation, relying on the omnidirectional affine formation mechanism, sequentially passed through two red hoops, with the white arrows in the diagram indicating the direction of movement through the hoops. The six sub-figures in Fig. 11 record critical moments of crossing the hoop. At  $t = 0s$ , marking the start of the movement, the formation first moves left and then forward to pass through the left hoop. In order to pass through the red hoop smoothly, the formation transforms into a straight line at  $t = 5s$ , applying affine transformations. It successfully passes through the left red hoop at  $t = 15s$ , returning to the regular pentagonal formation and completing the hierarchical reorganization. Subsequently, the formation reaches the front of the right red hoop at  $t = 20s$  and transforms into a straight line again at  $t = 25s$

to pass through the hoop. Finally, the formation returns to the original position at  $t = 45s$ .

The velocity distribution of the formation in Exp. 3 is shown in Fig. 13. In this experiment, the maximum instantaneous velocity of the formation is  $1.05m/s$ , with the largest velocity difference within the formation being  $1.04m/s$  and the smallest being  $0.46m/s$ . As shown in Fig. 13, compared with Exps. 1 and 2, in the phases of  $t = [5 - 10s, 15 - 20s, 25 - 30s, 35 - 40s]$  in Exp. 3, there are instances where the maximum velocity difference within the formation exceeds the maximum instantaneous velocity. This phenomenon corresponds to the radial formation transformation process, as depicted in Fig. 11. This indicates that during affine transformations, the relative velocities of drones within the formation change, resulting in inter-swarm movements towards each other.

The real drone trajectories and the formation center tracking error in Exp. 3 are shown in Fig. 12(a), which indicates that the formation undergoes dynamic leader switches after crossing through the hoops to complete the turn-around maneuver of the group successfully. Additionally, the tracking error of the formation center trajectory is relatively larger at the beginning of the affine transformation. To analyze the individual drone trajectory tracking error, Table VI records the tracking errors and the formation shape transformation matrix. Compared to Exps. 1 and 2, the individual drone tracking errors in Exp. 3 are relatively

more minor, which might be due to the comparatively lower movement speed of the formation in Exp. 3. Furthermore, Fig. 12(b) presents the expected and actual position curves for the  $x$  and  $y$  directions of different drones in Exp 3. It can be observed that the actual position curves consistently lag behind the expected value curves, consistent with the results of Exps. 1 and 2.

In the experiment involving dense formation changes, as shown in Fig 14, referred to as Exp. 4, five drones are arranged in a regular pentagon with a side length of  $1.2m$ . The formation undergoes continuous hierarchical reorganizations in the environment depicted in Fig. 7(c). The velocity distribution of the formation in Exp. 4 is shown in Fig. 15, with the maximum instantaneous speed within the formation being  $1.92m/s$ .

Table VII reflects the hierarchical reorganization scenario and transformation matrices at times labeled in Subfigures of Fig. 14. Combining the information from Fig. 14 and Table VII, it can be observed that at  $t = 3.1s, 14.3s$ , the formation changes into a straight line, at  $t = 0s, 13.3s, 19.1s$ , the formation undergoes scaling, at  $t = 6.3s, 21.2s$ , it expands, and at  $t = 3.1s, 6.3s, 13.3s$ , a dynamic leader switch occurs to respond to rapid maneuvers, such as a formation turning. Exp. 4 illustrates that affine transformations under hierarchical reorganization enable flexible transformations and rapid execution of complex maneuvers, such as formation U-turns.

## VI. CONCLUSION AND DISCUSSION

This work presents an innovative omnidirectional affine formation approach that leverages hierarchical reorganizations to improve aerial swarms' flexibility and in-team coordination. The efficacy of the proposed methodologies is verified through a series of simulations and extensive real-world trials, which indicate a significant enhancement in team flexibility. Specifically, the formation adeptly executes multiple hierarchical reorganizations, with the most prolonged reconfiguration completed in a mere  $0.047s$ . This rapid adaptability enables a quintet of aerial robots to undertake intricate, collaborative tasks, including executing agile maneuvers and navigating through obstacles at speeds reaching  $1.9m/s$ .

Future works will consider two main points. First, we intend to delve deeper into the control characteristics during the hierarchical reorganization process. This will allow us to enhance the robustness of formation control while maintaining high flexibility. Second, we will seek optimal points for dynamic leader autonomous switching, aiming to increase the autonomy of omnidirectional affine formation.

## REFERENCES

- [1] J. Hu, P. Bhowmick, I. Jang, F. Arvin, and A. Lanzon, "A decentralized cluster formation containment framework for multirobot systems," *IEEE Transactions on Robotics*, vol. 37, no. 6, pp. 1936–1955, Dec. 2021, conference Name: IEEE Transactions on Robotics.
- [2] X. Zhou, X. Wen, Z. Wang, Y. Gao, H. Li, Q. Wang, T. Yang, H. Lu, Y. Cao, C. Xu, and F. Gao, "Swarm of micro flying robots in the wild," *Science Robotics*, vol. 7, no. 66, p. eabm5954, 2022.
- [3] M. Abdelkader, S. Guler, H. Jaleel, and J. Shamma, "Aerial swarms: Recent applications and challenges," *Current Robotics Reports*, vol. 2, pp. 1–12, Sep. 2021.
- [4] L. Merino, F. Caballero, J. R. Martínez-de Dios, I. Maza, and A. Ollero, "An unmanned aircraft system for automatic forest fire monitoring and measurement," *J Intell Robot Syst*, vol. 65, no. 1, pp. 533–548, Jan. 2012.
- [5] X. Dong, B. Yu, Z. Shi, and Y. Zhong, "Time-varying formation control for unmanned aerial vehicles: Theories and applications," *IEEE Transactions on Control Systems Technology*, vol. 23, no. 1, pp. 340–348, Jan. 2015.
- [6] D. Yu, J. Long, C. L. Philip Chen, and Z. Wang, "Bionic tracking-containment control based on smooth transition in communication," *Information Sciences*, vol. 587, pp. 393–407, Mar. 2022.
- [7] D. Zhou, Z. Wang, and M. Schwager, "Agile coordination and assistive collision avoidance for quadrotor swarms using virtual structures," *IEEE Trans. Robot.*, vol. 34, no. 4, pp. 916–923, Aug. 2018.
- [8] S. Zhao, "Affine formation maneuver control of multiagent systems," *IEEE Trans. Automat. Contr.*, vol. 63, no. 12, pp. 4140–4155, Dec. 2018.
- [9] D. Mateo, Y. K. Kuan, and R. Bouffanais, "Effect of correlations in swarms on collective response," *Sci Rep*, vol. 7, no. 1, p. 10388, Sep. 2017.
- [10] A. Attanasi, A. Cavagna, L. Del Castello, I. Giardina, T. S. Grigera, A. Jelić, S. Melillo, L. Parisi, O. Pohl, E. Shen, and M. Viale, "Information transfer and behavioural inertia in starling flocks," *Nature Phys.*, vol. 10, no. 9, pp. 691–696, Sep. 2014.
- [11] K. Chen, W. He, Q.-L. Han, M. Xue, and Y. Tang, "Leader selection in networks under switching topologies with antagonistic interactions," *Automatica*, vol. 142, p. 110334, Aug. 2022.
- [12] W. Luo, S. S. Khatib, S. Nagavalli, N. Chakraborty, and K. Sycara, "Distributed knowledge leader selection for multi-robot environmental sampling under bandwidth constraints," in *2016 IEEE/RSJ International Conference on Intelligent Robots and Systems (IROS)*, 2016, pp. 5751–5757.
- [13] A. Clark, B. Alomair, L. Bushnell, and R. Poovendran, "Leader selection in multi-agent systems for smooth convergence via fast mixing," in *2012 IEEE 51st IEEE Conference on Decision and Control (CDC)*, 2012, pp. 818–824.
- [14] F. Xiao, Q. Yang, X. Zhao, and H. Fang, "A framework for optimized topology design and leader selection in affine formation control," *IEEE Robotics and Automation Letters*, vol. 7, no. 4, pp. 8627–8634, 2022.
- [15] A. Franchi, H. H. Bühlhoff, and P. Robuffo Giordano, "Distributed online leader selection in the bilateral teleoperation of multiple UAVs," in *2011 50th IEEE Conference on Decision and Control and European Control Conference*, Dec. 2011, pp. 3559–3565.
- [16] S. Misra, P. K. Deb, and K. Saini, "Dynamic leader selection in a master-slave architecture-based micro uav swarm," in *2021 IEEE Global Communications Conference (GLOBECOM)*, 2021, pp. 1–6.
- [17] M. A. Abdel-Malek, K. Akkaya, A. Bhuyan, and A. S. Ibrahim, "A proxy signature-based swarm drone authentication with leader selection in 5g networks," *IEEE Access*, vol. 10, pp. 57 485–57 498, 2022.
- [18] R. Ganesan, X. M. Raajini, A. Nayyar, P. Sanjeevikumar, E. Hossain, and A. H. Ertas, "BOLD: Bio-inspired optimized leader election for multiple drones," *Sensors*, vol. 20, no. 11, p. 3134, Jan. 2020, number: 11 Publisher: Multidisciplinary Digital Publishing Institute.
- [19] H. Saeidi, D. G. Mikulski, and Y. Wang, "Trust-based leader selection for bilateral haptic teleoperation of multi-robot systems," in *2017 IEEE/RSJ International Conference on Intelligent Robots and Systems (IROS)*, Sep. 2017, pp. 6575–6581.
- [20] A. d. H. B. M. Tavares, S. P. Madruga, A. V. Brito, and T. P. Nascimento, "Dynamic leader allocation in multi-robot systems based on nonlinear model predictive control," *J Intell Robot Syst*, vol. 98, no. 2, pp. 359–376, May 2020.
- [21] F. Li, Y. Ding, M. Zhou, K. Hao, and L. Chen, "An affection-based dynamic leader selection model for formation control in multirobot systems," *IEEE Transactions on Systems, Man, and Cybernetics: Systems*, vol. 47, no. 7, pp. 1217–1228, Jul. 2017.

- [22] M. Nagy, Z. Ákos, D. Biro, and T. Vicsek, "Hierarchical group dynamics in pigeon flocks," *Nature*, vol. 464, no. 7290, pp. 890–893, 2010.
- [23] Z. Chen, H.-T. Zhang, X. Chen, D. Chen, and T. Zhou, "Two-level leader-follower organization in pigeon flocks," *Europhysics Letters*, vol. 112, no. 2, p. 20008, nov 2015.
- [24] Y. Cao, W. Yu, W. Ren, and G. Chen, "An overview of recent progress in the study of distributed multi-agent coordination," *IEEE Transactions on Industrial Informatics*, vol. 9, no. 1, pp. 427–438, 2013.
- [25] K.-K. Oh, M.-C. Park, and H.-S. Ahn, "A survey of multi-agent formation control," *Automatica*, vol. 53, pp. 424–440, 2015.
- [26] S.-M. Kang, M.-C. Park, B.-H. Lee, and H.-S. Ahn, "Distance-based formation control with a single moving leader," in *2014 American Control Conference*, 2014, pp. 305–310.
- [27] R. Babazadeh and R. Selmic, "An optimal displacement-based leader-follower formation control for multi-agent systems with energy consumption constraints," in *2018 26th Mediterranean Conference on Control and Automation (MED)*, 2018, pp. 179–184.
- [28] S.-L. Dai, S. He, H. Cai, and C. Yang, "Adaptive leader-follower formation control of underactuated surface vehicles with guaranteed performance," *IEEE Transactions on Systems, Man, and Cybernetics: Systems*, vol. 52, no. 3, pp. 1997–2008, Mar. 2022.
- [29] X. Fang, X. Li, and L. Xie, "Distributed formation maneuver control of multiagent systems over directed graphs," *IEEE Transactions on Cybernetics*, vol. 52, no. 8, pp. 8201–8212, Aug. 2022.
- [30] Y. Nomura, H. Fukushima, and F. Matsuno, "Navigation of multiple UAVs in 3d obstacle environments while preserving connectivity without data transmission," in *2021 IEEE Conference on Control Technology and Applications (CCTA)*, Aug. 2021, pp. 82–89.
- [31] M. Porfiri, D. G. Roberson, and D. J. Stilwell, "Tracking and formation control of multiple autonomous agents: A two-level consensus approach," *Automatica*, vol. 43, no. 8, pp. 1318–1328, 2007.
- [32] G. Droge, "Distributed virtual leader moving formation control using behavior-based mpc," in *2015 American Control Conference (ACC)*, 2015, pp. 2323–2328.
- [33] Z. Lin, L. Wang, Z. Chen, M. Fu, and Z. Han, "Necessary and sufficient graphical conditions for affine formation control," *IEEE Transactions on Automatic Control*, vol. 61, no. 10, pp. 2877–2891, 2016.
- [34] D. Li, G. Ma, Y. Xu, W. He, and S. S. Ge, "Layered affine formation control of networked uncertain systems: A fully distributed approach over directed graphs," *IEEE Transactions on Cybernetics*, vol. 51, no. 12, pp. 6119–6130, Dec. 2021.
- [35] Y. Xu, D. Li, D. Luo, and Y. You, "Affine formation maneuver tracking control of multiple second-order agents with time-varying delays," *Sci. China Technol. Sci.*, vol. 62, no. 4, pp. 665–676, Apr. 2019.
- [36] M. Wang and T. Zhang, "Leader-following formation control of second-order nonlinear systems with time-varying communication delay," *Int. J. Control Autom. Syst.*, vol. 19, no. 5, pp. 1729–1739, May 2021.
- [37] S. Luo, X. Xu, L. Liu, and G. Feng, "Leader-following consensus of heterogeneous linear multiagent systems with communication time-delays via adaptive distributed observers," *IEEE Transactions on Cybernetics*, vol. 52, no. 12, pp. 13 336–13 349, Dec. 2022.
- [38] J. Wang, X. Ding, C. Wang, L. Liang, and H. Hu, "Affine formation control for multi-agent systems with prescribed convergence time," *Journal of the Franklin Institute*, vol. 358, no. 14, pp. 7055–7072, Sep. 2021.
- [39] X. Yu, D. Saldaña, D. Shishika, and M. A. Hsieh, "Resilient consensus in robot swarms with periodic motion and intermittent communication," *IEEE Transactions on Robotics*, vol. 38, no. 1, pp. 110–125, 2022.
- [40] T. Zhao, D. Cao, J. Yao, and S. Zhang, "Topology optimization algorithm for UAV formation based on wireless ultraviolet communication," *Photon Netw Commun*, vol. 45, no. 1, pp. 25–36, Feb. 2023.
- [41] D. Yu and C. L. P. Chen, "Smooth transition in communication for swarm control with formation change," *IEEE Transactions on Industrial Informatics*, vol. 16, no. 11, pp. 6962–6971, 2020.
- [42] M. Mesbahi and M. Egerstedt, *Graph theoretic methods in multiagent networks*. Princeton University Press, 2010.
- [43] R. Olfati-Saber, J. A. Fax, and R. M. Murray, "Consensus and cooperation in networked multi-agent systems," *Proceedings of the IEEE*, vol. 95, no. 1, pp. 215–233, 2007.
- [44] X. Dong, Y. Zhou, Z. Ren, and Y. Zhong, "Time-varying formation tracking for second-order multi-agent systems subjected to switching topologies with application to quadrotor formation flying," *IEEE Transactions on Industrial Electronics*, vol. 64, no. 6, pp. 5014–5024, 2017.
- [45] Y. Zou, Z. Zhou, X. Dong, and Z. Meng, "Distributed formation control for multiple vertical takeoff and landing uavs with switching topologies," *IEEE/ASME Transactions on Mechatronics*, vol. 23, no. 4, pp. 1750–1761, 2018.
- [46] B. Liu, T. Chu, L. Wang, and G. Xie, "Controllability of a leader-follower dynamic network with switching topology," *IEEE Transactions on Automatic Control*, vol. 53, no. 4, pp. 1009–1013, 2008.
- [47] J.-L. Wang and H.-N. Wu, "Leader-following formation control of multi-agent systems under fixed and switching topologies," *International Journal of Control*, vol. 85, no. 6, pp. 695–705, 2012.
- [48] S. K. Soni, A. Sachan, S. Kamal, S. Ghosh, and M. Djemai, "Leader-following formation control of second-order autonomous unmanned systems under switching topologies," in *2021 60th Annual Conference of the Society of Instrument and Control Engineers of Japan (SICE)*, 2021, pp. 779–784.
- [49] R. Connelly, "Generic global rigidity," *Discrete Comput Geom*, vol. 33, no. 4, pp. 549–563, Apr. 2005.



**Yuzhu Li** received a B.Sc. degree in aircraft manufacturing engineering from Tongji University, Shanghai, China, in 2020. She is currently a Ph.D. candidate in the School of Mechanical Engineering, Shanghai Jiao Tong University. Her research interests include cooperative localization and the intelligent control of unmanned systems.



**Wei Dong** received a B.S. degree and Ph.D. in mechanical engineering from Shanghai Jiao Tong University, Shanghai, China, in 2009 and 2015, respectively. He is currently an associate professor in the School of Mechanical Engineering, Shanghai Jiao Tong University. His research interests include the cooperation, perception, and agile control of unmanned systems.